Actin filaments growing against a barrier with fluctuating shape

Raj Kumar Sadhu and Sakuntala Chatterjee

Department of Theoretical Sciences, S. N. Bose National Centre for Basic Sciences, Block JD, Sector III,
Salt Lake, Kolkata 700106, India

We study force generation by a set of parallel actin filaments growing against a nonrigid obstacle, in the presence of an external load. The filaments polymerize by either moving the whole obstacle, with a large energy cost, or by causing local distortion in its shape which costs much less energy. The nonrigid obstacle also has local thermal fluctuations due to which its shape can change with time and we describe this using fluctuations in the height profile of a one-dimensional interface with Kardar-Parisi-Zhang dynamics. We find the shape fluctuations of the barrier strongly affect the force generation mechanism. The qualitative nature of the force-velocity curve is crucially determined by the relative time scale of filament and barrier dynamics. The height profile of the barrier also shows interesting variation with the external load. Our analytical calculations within mean-field theory show reasonable agreement with our simulation results.

I. INTRODUCTION

Cell motility plays an important role in a wide variety of biological processes such as morphogenesis, wound healing, or tumor invasion [1–4]. Actins and microtubules are cytoskeletal proteins whose polymerization and depolymerization can generate significant forces, without any assistance of molecular motors, and propel the cell forward. In the presence of a biological barrier, these filaments elongate and generate a pushing force against the barrier and in many *in vitro* studies this force has been measured explicitly by applying an external load on the barrier in the opposite direction. With increasing load, the velocity of the barrier decreases and the functional nature of dependence of velocity on the applied force is an important characteristic of the force generation mechanism. The maximum polymerization force generated by the filaments is known as "stall force" and is measured as the minimum load required in order to stall the barrier motion completely. There has been a surge of experimental as well as theoretical research activities to determine the stall force and the force-velocity characteristic of the cytoskeletal filaments in the last few years.

Interestingly, the qualitative nature of the force-velocity curve was found to depend on the details of the experimental setup. A convex force-velocity characteristic was reported for actin quoted polystyrene beads [5] and magnetic colloidal particles pushed by unbranched parallel actin filaments [6,7]. On the other hand, a concave force-velocity curve was obtained for branched actin network [8], where velocity remains almost constant for small load and drops rapidly at large load. An even more complex force-velocity relationship was measured for lamellipodial protrusion in a keratocyte, where velocity showed rapid decay for very small load, followed by a plateau at moderate load and another rapid decay close to stalling [9,10]. Although multiple filaments are expected to generate larger force than a single filament [5,9,11], in [12] the stall force of approximately eight actin filaments was measured and found to be in the piconewton range, close to a single filament stall force [13], indicating the absence of cooperation among the filaments.

To investigate the force-velocity relationship theoretically, several different models have been proposed. Force generation by a single actin filament growing against a barrier has

been explained using a simple Brownian ratchet mechanism where thermal fluctuations of the barrier create a gap between the barrier and the filament tip, making it possible for the filament to grow by adding one monomer in the gap [14]. This mechanism predicts a convex force-velocity curve. This simple model has been subsequently generalized where details of interaction between the monomers and the barrier have been considered [15] and flexibility of the filament has been included [16]. In all these cases the existence of a convex force-velocity relationship has been verified. However, when the Brownian ratchet mechanism was extended for multiple filaments, the nature of the force-velocity curve was found to crucially depend on how the details of the interaction and load sharing among the filaments were modeled [17–20]. Certain models even showed a crossover from convex to concave force-velocity curve, as some model parameters are varied [21–23].

Inside a cell, actin filaments grow against the plasma membrane which is not a rigid object but elastically deformable [24]. Even *in vitro*, when the filaments push against an obstacle as they polymerize, the obstacle may in general have local shape deformations. In [25] a flexible plasma membrane was explicitly modeled and it was shown that thermal fluctuation of this flexible obstacle substantially enhances the growth velocity of a filopodial protrusion. It was argued that in the case of a flexible membrane, a filament only has to overcome the local bending energy in order to polymerize (whereas for a rigid obstacle the full load must be overcome) and this gives rise to a larger velocity for a given load. The effect of a flexible plasma membrane on actin network growth was experimentally demonstrated in [26] when reconstituted actin networks *in vitro* were assembled onto synthetic lipid bilayers and it was found that the membrane elasticity causes formation of bundled filament protrusion from branched filament networks.

Motivated by this, we carry out a study to probe the detailed quantitative aspects of interaction between a set of growing filaments and an obstacle whose position as well as shape can fluctuate with time. To keep our description simple, we model the obstacle by a one-dimensional nonrigid object whose local thermal fluctuations can alter its shape and using

a lattice gas model, we describe it by a Kardar-Parisi-Zhang (KPZ) interface [27]. In the presence of an external load, the obstacle tends to move in the direction opposite to that of polymerization. In order to polymerize, the filaments must push against the barrier, either causing a local change in its profile (which requires less energy) or causing a global movement of the whole barrier (which involves a large energy cost). We are interested to find out how the presence of the fluctuating barrier affects the dynamics of the actin filaments, and how the presence of the filaments affects the shape of the barrier.

Our numerical simulations and analytical calculations show that there is a rich interplay between the polymerization dynamics of the filaments and the shape fluctuations of the barrier. For small and intermediate values of the external force, the barrier motion is governed by its global movement, and for large force, the local fluctuations become important. These local movements cost less energy and can continue even when the force is significantly large. As a result, the stall force in our system is much higher than that for a rigid barrier [18]. Moreover, these local movements may be caused by filament polymerization or by independent thermal fluctuations of the barrier and hence the stall force may also depend on the properties of the barrier. Indeed for a single filament, the stall force is found to increase with the size of the barrier. For N filaments stall force is independent of the barrier size and scales linearly with N. The barrier shape is also affected by the growing filaments and the scaling behavior of its height profile shows continuous variation as a function of the external load.

There are two time scales in our system, one associated with the (de)polymerization of the filaments and the other with the thermal fluctuations of the barrier. Our results show that the choice of these time scales may crucially determine the nature of the force-velocity curve. This is because the local movements of the barrier make an increasingly important contribution to its velocity as the thermal fluctuations become faster. Even for small or intermediate load, therefore, the barrier velocity is not governed by its global movement alone and this changes the qualitative nature of dependence of velocity on load. The stall force is also found to decrease for faster barrier dynamics.

This paper is organized as follows. In Sec. II, we describe our model. Our results for the single filament and multiple filaments are presented in Secs. III and IV, respectively, and conclusions are in Sec. V.

II. DESCRIPTION OF THE MODEL

Our model consists of N parallel filaments growing against a barrier with a fluctuating height profile (see Fig. 1). We model the filaments as rigid polymers, made of rodlike monomers of length d, such that a (de)polymerization event (decreases) increases the length of the filament by an amount d. The barrier is modeled as a one-dimensional surface. In our lattice model, the discrete surface elements are represented as lattice bonds of length λ, which can have two possible orientations, $\pm\pi/4$. We denote these two cases by the symbols / and \ and call them upslope and downslope bonds, respectively. Height at

any particular lattice site i is defined as $h_i = \delta/2 \sum_{j=1}^{i-1} \tan\theta_j$, where θ_j is the orientation of the jth bond and $\delta = \sqrt{2}\lambda$. The total number of such bonds is L. One / followed by a \ forms a local hill and in the reverse order \/ they form a local valley. The local height of the surface fluctuates due to transition between these hills and valleys. When a local hill (valley) at a given site flips to a valley (hill), the height of that particular site decreases (increases) by an amount δ. We assume δ is equal to the monomer length d. As explained below, this assumption means that height fluctuation of the surface creates a gap which is just enough for insertion of a monomer. Towards the end of the paper, we briefly discuss the case of $\delta \neq d$.

A filament whose tip is in contact with the barrier is called a bound filament and in the absence of any such contact, it is called a free filament. The surface site where a bound filament can form a contact is called a binding site. When a bound filament polymerizes, it creates space for insertion of another monomer by pushing the barrier up and in this process performs work against the external load (which tends to push the barrier down). When the bound filament pushes against a local valley, that valley flips to a hill and the height of the binding site increases by an amount d [Fig. 1(a)]. However, polymerization of a bound filament, which is not in contact with a local valley, requires a global movement of the whole barrier as shown in Fig. 1(b), when heights of all the L sites are increased by an amount d. Assuming F/L is the load per site, the energy cost for the first process is just Fd/L, and for the second process it is Fd. Following the rule of local detailed balance, we assign rates $U_0 \exp(-\beta Fd/L)$ and $U_0 \exp(-\beta Fd)$ to these two types of polymerization processes, respectively. Here, β is the inverse temperature and U_0 is the free filament polymerization rate that does not involve any barrier movement and hence is independent of F. We also assume the depolymerization rate is same for both free and bound filaments and is denoted as W_0. When a bound filament depolymerizes, it loses contact with the barrier and becomes a free filament. In certain configurations, when there is only one bound filament, its depolymerization results in an unsupported barrier.

Apart from being pushed by the filaments, the barrier can also show thermal fluctuations, when local hills can flip to valleys and vice versa. However, due to the presence of the filaments, these transitions can sometimes get blocked. For example, if a bound filament is in contact with a hill, then that particular hill cannot flip to a valley, until the filament depolymerizes and a gap is created for a local downward movement of the barrier. When both forward and reverse transitions are allowed, their rates satisfy local detailed balance $\frac{R_+}{R_-} = e^{-\beta Fd/L}$, where R_+ is the rate at which local surface height can increase (i.e., a valley flips to a hill) and R_- is the reverse transition rate. Note that in the absence of any external load F, the transition between hills and valleys become symmetric at all sites other than the binding sites and the surface has a local Edwards-Wilkinson dynamics [28]. For nonzero F, hill to valley transitions are generally favored (except, possibly, at the binding site) and the barrier behaves like a KPZ surface with a downward bias.

We assume periodic boundary conditions for the surface and an equal number of upslope and downslope bonds, i.e., no
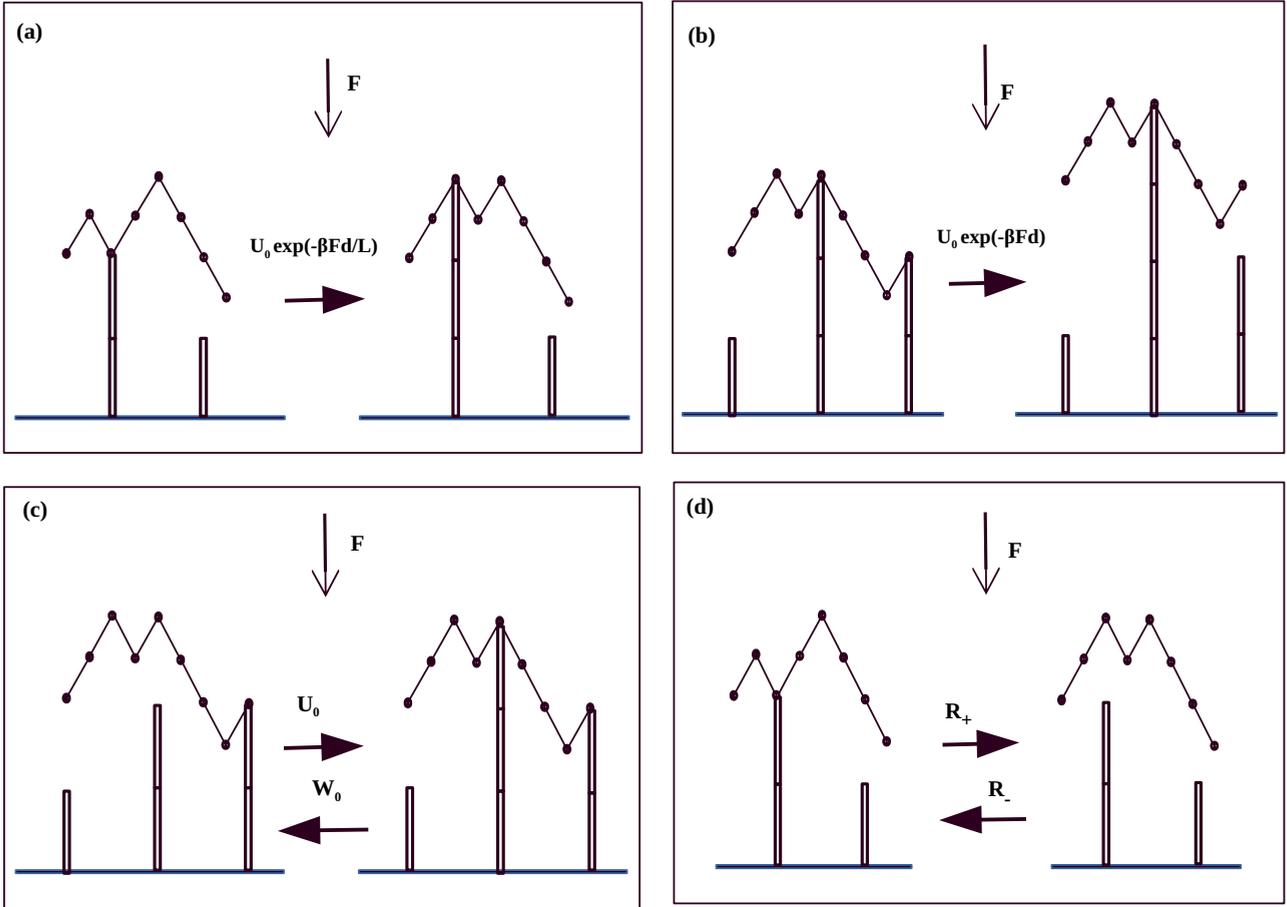
FIG. 1. Schematic representation of our model. (a) Polymerization of a bound filament by causing a local change in barrier height with rate $U_0 e^{-\frac{\beta F d}{L}}$. (b) A bound filament polymerizes by causing global movement of the whole barrier with rate $U_0 e^{-\beta F d}$. (c) A free filament polymerizes and depolymerizes with rates U_0 and W_0, respectively. Since these processes do not involve any barrier motion, these rates are independent of F. (d) Thermal fluctuation of the barrier: a local valley can flip to a hill with rate R_+ and the reverse process occurs with rate R_-. We use local detailed balance, $R_+/R_- = \exp(-\beta F d/L)$, except at the binding sites, where hill to valley transition may be blocked due to the presence of a filament.

overall tilt. In one Monte Carlo step, we attempt to perform N filament updates (polymerization or depolymerization) and S independent (unaided by the filaments) surface updates. By changing the value of S we can tune the relative time scale between filament dynamics and barrier dynamics. For smaller (larger) S value, the barrier dynamics is slower (faster) than the filament dynamics. A relative time scale between the surface and filament dynamics can also be introduced by rescaling R_+ and R_-, but we have used $R_- = U_0$ and $R_+ = U_0 e^{-\beta F d/L}$ throughout and controlled the relative time scale by S instead. We start with an initial configuration where all N filaments have unit length, containing one monomer each and the upslope and downslope bonds are placed alternatingly (a flat surface). We let the system evolve for a long time, according to the above dynamical rules. All our measurements are performed in the steady state.

III. RESULTS FOR SINGLE FILAMENT

For a single filament, we first present the results for $S = L$ and later we consider the effect of variation of S. We define the velocity V of the barrier as the rate of change of the

average height of the surface after the system has reached steady state. We present the force-velocity curve in Fig. 2(a). This curve has a convex shape where velocity decays rapidly for small force, and for large force it decays slowly. In fact for small and intermediate values of force, the velocity falls off exponentially [Fig. 2(a), inset] and close to stalling it shows deviation from the exponential form. We explain below that the exponential dependence originates from the global movement of the barrier [as shown in Fig. 1(a)] which dominates V for small and moderate F range. In Fig. 2(b) we show the variation of stall force F_s with the barrier size L. Stall force increases with L, although logarithmically slowly. Note that the stall force is often interpreted as the maximum polymerization force generated by the filament and therefore it is somewhat surprising that it depends on the size of the barrier. We show below that in our system the local fluctuations of the barrier, which depend on L, make substantial contribution towards its net velocity and this becomes particularly significant in the stalling regime.

In our system there are two possible barrier movements: global and local. In a global movement, a bound filament polymerizes by pushing the whole barrier up, such that the
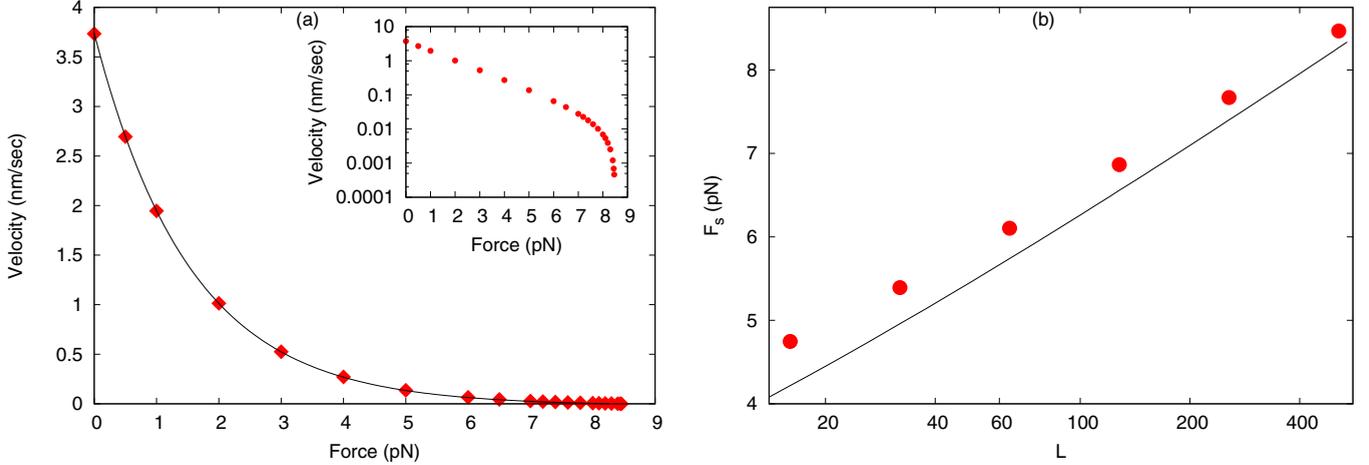
FIG. 2. Force-velocity characteristic and stall force for a single filament. (a) Force-velocity curve has a convex shape. Inset shows exponential decay of the barrier velocity for small and intermediate F, when the global motion of the barrier dominates. Close to stalling the local fluctuations become important. We have used $L = 512$ here. (b) Stall force increases with the barrier size L. In both the panels, we have used $S/L = 1$. The free filament depolymerization rate $W_0 = 1.4$ s^{-1} [1,29] and the polymerization rate U_0 is proportional to the free monomer concentration with a proportionality constant $k_0 = 11.6$ μm^{-1} s^{-1} [1,29]. We have used a monomer concentration $C = 0.24$ μm, which gives $U_0 = 2.784$ s^{-1}. The monomer size is $d = 2.7$ nm [1,23]. At room temperature the parameter $\beta d = 0.65$ pN^{-1}. Discrete points show simulation data and continuous lines show analytical results.

average height changes by an amount d. The rate at which this process happens is $U_0 \exp(-\beta F d)$. Let this process contribute a velocity V_1 to the barrier in steady state, which can be written as

$$V_1 = p_0 d U_0 \exp(-\beta F d). \tag{1}$$

Here, p_0 is the probability that the filament is in contact with the barrier. Note that here we have ignored the possibility that the bound filament is pushing against a valley (in that case no global movement takes place; only a local flip is sufficient for polymerization). In fact we have verified in our simulation [data presented in Fig. 6(b)] that the probability of finding a valley at the binding site is indeed small.

To write V_1 as a function of F we still need to calculate p_0. Define p_i as the probability that the distance between the filament tip and the binding site is i. Clearly, $i = 0$ corresponds to the contact probability. It is easy to see that for $i > 0$, the probability p_i satisfies the master equation for a biased random walker,

$$\frac{dp_i}{dt} = W_0 p_{i-1} + U_0 p_{i+1} - (W_0 + U_0) p_i, \tag{2}$$

and for $i = 0$ one has

$$\frac{dp_0}{dt} = U_0 p_1 - W_0 p_0. \tag{3}$$

Here, we have ignored any change in p_i due to height fluctuations at the binding site. For fast barrier dynamics, when height fluctuations increase, this assumption breaks down. In the steady state, these equations yield a recursion relation $p_i = (\frac{W_0}{U_0})^i p_0$ for positive i. This recursion relation, along with the normalization condition $\sum_i p_i = 1$, yields the expression $p_0 = (1 - W_0/U_0)$, which is independent of F. So the final expression for V_1 becomes

$$V_1 = d(U_0 - W_0) \exp(-\beta F d). \tag{4}$$

To calculate the velocity due to local height fluctuations of the barrier, we consider a local valley (hill) flipping to a hill (valley) which increases (decreases) the average height by an amount d/L. As discussed in Sec. II, the transition rates at the binding site are different from the rest of the system, since a hill to valley transition may be blocked, if a filament is in contact. Then the barrier velocity due to local height fluctuations can be written as

$$V_2 = \frac{dU_0}{L}\left[\left((1 + p_0)p_v(0) + \sum_{i=1}^{L-1} p_v(i)\right)e^{-\beta F d/L} \right.$$
$$\left. - (1 - p_0)p_h(0) - \sum_{i=1}^{L-1} p_h(i)\right], \tag{5}$$

where $p_v(i)$ and $p_h(i)$ denote the probability to find a valley and a hill, respectively, at a distance i from the binding site. In the above equation, the first term on the right-hand side represents the situation where a valley at the binding site flips to a hill, due to thermal fluctuations or due to being pushed by the filament. The second term presents flipping of a valley to a hill at all the other sites. The third term describes the case when there is a hill at the binding site which can flip to a valley when no filament is in contact. The fourth term describes flipping of a hill to a valley in the rest of the system. The probabilities $p_v(i)$ and $p_h(i)$ can be calculated within a mean-field approximation by considering a KPZ surface with the binding site acting as a "defect site" (see Appendix A for details), where the transition rates are different from the rest of the system. Our calculations show that $p_v(i)$ and $p_h(i)$ have a rather weak dependence on F and their difference $[p_v(i) - p_h(i)]$ is independent of i and scales as $1/L$. For large L, the total velocity of the barrier

$V = V_1 + V_2$ can be written as

$$V(F) = d(U_0 - W_0)e^{-\beta F d}$$

$$+ \frac{dU_0}{L}\left[p_v(0)(1 + p_0) - (1 - p_0)p_h(0) \right.$$

$$\left. + \sum_{i=1}^{L-1} \left\{ p_v(i)\left(1 - \frac{\beta d F}{L}\right) - p_h(i) \right\} \right], \quad (6)$$

where we have retained terms up to order $1/L$ and ignored higher order terms. In Fig. 2(a) we compare our calculation with simulation results and obtain reasonably good agreement. For small F, the first term in Eq. (6) dominates the velocity and as F increases, local fluctuations become more important. The last term in Eq. (6), within the braces, which represents the velocity due to hill-valley fluctuations at all sites, except the binding site, is the most dominant term in the local movement. In the stalling region, the positive contribution from the global movement and the negative contribution from the local fluctuations cancel each other, where the first and last terms of Eq. (6) determine the major balance. The stall force F_s can be obtained by graphically solving the above transcendental equation after putting its left-hand side zero. This gives stall force as a function of L and we compare this variation with simulation results in Fig. 2(b). We find good agreement for large L but as expected, for small L there are deviations. Note that the stall force in our system is substantially higher than that for a rigid barrier [18]. Since the local movements cost much less energy, they can continue even when the load is high.

A. Effect of faster and slower barrier dynamics

We find the nature of the force-velocity curve depends on the relative time scale of the barrier and filament dynamics. For faster barrier dynamics, the local fluctuations of the barrier increase and as a result their contribution to the net velocity is also higher. This means even for small force, the velocity is not dominated by the global movement [first term in Eq. (6)] alone. In addition, our simple expression for the contact probability $p_0 = (1 - W_0/U_0)$, which was derived neglecting the local fluctuations at the binding site, does not remain valid for fast barrier dynamics and p_0 increases with F in this case (see our data in Fig. 7). As a result, the velocity does not decay exponentially for small force, but follows a slower decay. For a given value of F in the small or intermediate range, as the barrier dynamics becomes faster, the velocity becomes higher, and the convex nature of the curve is gradually lost. Moreover, since stalling phenomenon in our system can be described as a balance between global and local velocities of the barrier [see Eq. (6)], larger contribution from local movement implies this balance is reached at a smaller value of force. Therefore, for faster barrier dynamics we have a smaller stall force. We present our data in Figs. 3(a) and 3(b).

Our data in Fig. 3(b) imply that in the limit of infinitely slow barrier dynamics, when the barrier can be considered as an effectively rigid object, the stall force diverges. Note that even in this limit, our model remains different from the rigid barrier case studied in [18], where at least one filament is always bound to the barrier. For $N = 1$ this would mean whenever there is a depolymerization, the barrier also moves down, along with the filament tip. On the contrary, we allow unsupported barrier in our system and when the barrier is effectively rigid, it shows only global movement which is always in the upward direction. The force velocity curve is perfectly exponential in this case and zero velocity is reached at the $F \to \infty$ limit.

B. Variation of the shape of the barrier with load

We have seen above how the barrier fluctuations affect the growth of the filament. The barrier properties are also altered in this process. As the load increases, the height profile
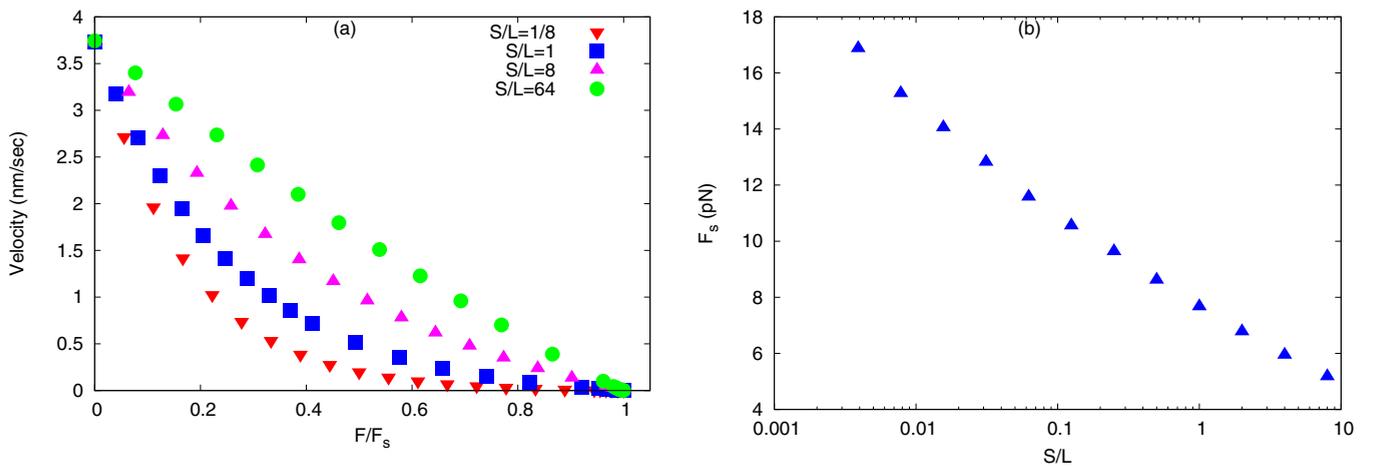
FIG. 3. Force-velocity characteristic for a single filament depends on the relative time scale between the filament and the barrier dynamics. (a) Velocity of the barrier vs scaled force for different values of S/L. For large S/L, the convex nature of the force-velocity characteristic is lost. As S/L increases, the local fluctuations of the barrier become more important and even for small F, the barrier velocity is not governed by the global movement alone, and hence V does not decay exponentially anymore. Here, we have used $L = 64$. (b) Stall force decreases as a function of S/L. Since local movements of the barrier become more important for large S/L, the balance between global and local movements is reached at a smaller force. Note, however, that the x axis is plotted in a log scale, indicating a weak dependence of stall force on the time scale. Here we have used $L = 256$. The other parameters are the same as in Fig. 2.
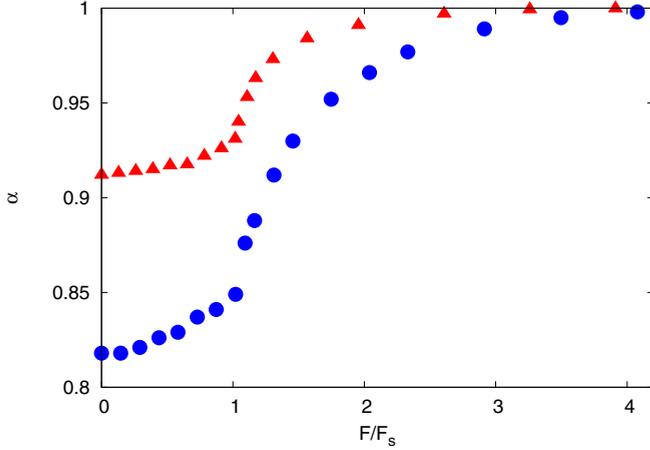
FIG. 4. Variation of α as a function of external load. Close to the stalling force, α shows a sharp increase. Here, we have used $S/L = 1$ and $L = 256$ (red triangle) and 128 (blue circle). Other simulation parameters are the same as in Fig. 2.

of the barrier shows larger variation across the system. We characterize it by measuring the scaling of average height with distance from the binding site: $\langle h(r) - h(0) \rangle \sim r^{\alpha}$, where $h(r)$ is the height of a site at a distance r from the binding site. In Fig. 4 we plot α as a function of the external force, which shows that for small force α increases slowly, around the stalling force there is a sharp increase, and finally for very large force, α saturates to unity. Note that large value of α indicates the presence of large hills and valleys in the system. $\alpha = 1$ corresponds to a phase separation of upslope and downslope bonds in the system which gives rise to one single large hill, the highest point being the binding site. This situation is similar to the case of an elastic membrane, when the membrane tension is large and the membrane is stretched.

IV. RESULTS FOR MULTIPLE FILAMENTS

In the case of N filaments in the system, we mainly consider the case when the ratio N/L is small. We assume the binding sites are uniformly placed on the lattice, at a distance L/N. Between the segment of two successive binding sites, the same considerations as in a single filament case apply. We assume these segments are independent and apply our results for the single filament case for each segment.

To start with, we consider the velocity of the barrier due to its global movement $V_1 = p_0 N d U_0 \exp(-\beta F d)$. As before, p_0 is the probability to find a filament in contact with the barrier and $p_0 N$ is the average number of bound filaments in the system. Here, we have neglected any correlation between the binding sites. To calculate p_0, we write down master equations for average number N_i of filaments at a distance i from the corresponding binding sites. The steady state solutions of these equations can be obtained recursively for different values of i (see Appendix C for details). For N filaments we have

$$p_0 = \frac{(1 - W_0/U_0)}{1 + (N - 1) \exp(-\beta F d)}. \quad (7)$$

For large F, the contact probability becomes the same as the single filament case. For small F, the contact probability is

approximately $1/N$ times the single filament value, indicating that for small F, at most one filament is in contact with the barrier.

For the local movement of the barrier, we need to calculate the probabilities to find hills and valleys. As discussed above, for each segment between two successive binding sites, we use our results for $p_v(i)$ and $p_h(i)$ for the single filament case [with the modification that i in this case varies from 0 to $(L/N - 1)$]. The velocity due to local fluctuations then becomes

$$V_2 = \frac{N d U_0}{L} \left[\left(p_v(0)(1 + p_0) + \sum_{i=1}^{L/N-1} p_v(i) \right) e^{-\beta F d/L} \right. $$
$$\left. - (1 - p_0) p_h(0) - \sum_{i=1}^{L/N-1} p_h(i) \right]. \quad (8)$$

The total velocity to leading order in $1/L$ and N/L becomes

$$V(F) = d \frac{(U_0 - W_0)}{1 + (N-1)e^{-\beta F d}} N e^{-\beta F d}$$
$$+ \frac{d U_0 N}{L} \left[\{ p_v(0)(1 + p_0) - p_h(0)(1 - p_0) \} \right.$$
$$\left. + \sum_{i=1}^{L/N-1} \left\{ p_v(i) \left(1 - \frac{\beta F d}{L} \right) - p_h(i) \right\} \right]. \quad (9)$$

The stall force can be obtained by solving the above transcendental equation graphically for $V(F) = 0$ and we compare the analytical stall force with our simulation results in Fig. 5(a), inset. We find that the stall force is independent of L in this case and scales with N, which can be easily seen from Eq. (9). Since the value of the stall force is rather large in this case, one can neglect global movement of the barrier close to the stalling regime. In addition, $p_0 \approx (1 - W_0/U_0)$ for large force, and $[p_v(i) - p_h(i)]$ is of order N/L. Using these in Eq. (9) it directly follows that the stall force for N filaments is independent of L and scales as N. We also investigate the effect of the time scale of the barrier dynamics on the force-velocity dependence [Fig. 5(b)] and we find qualitatively the same effect as in the $N = 1$ case.

V. CONCLUSIONS

In this paper, we have studied force generation by a set of parallel filaments polymerizing against a barrier. A similar question has been addressed in many recent works where the barrier was modeled as a rigid wall, which may have a motion like a thermal ratchet [14,15,30,31], or may be a passive obstacle which can move only when pushed by the filaments [18,20,23,32–34]. In this paper, we have considered a barrier with thermal fluctuations but instead of modeling it as a rigid wall, we allow for its shape fluctuations. In [35] a similar aspect was studied where the barrier was modeled by a one-dimensional Edwards-Wilkinson type membrane under tension, which was being locally pushed by a set of growing filaments. The uncorrelated drive from the filaments gives rise to a KPZ type behavior in the correlated height fluctuations of the membrane, but this is associated with very slow crossover. Interestingly, the steady-state fluctuations of the driven membrane show a nonmonotonic behavior with
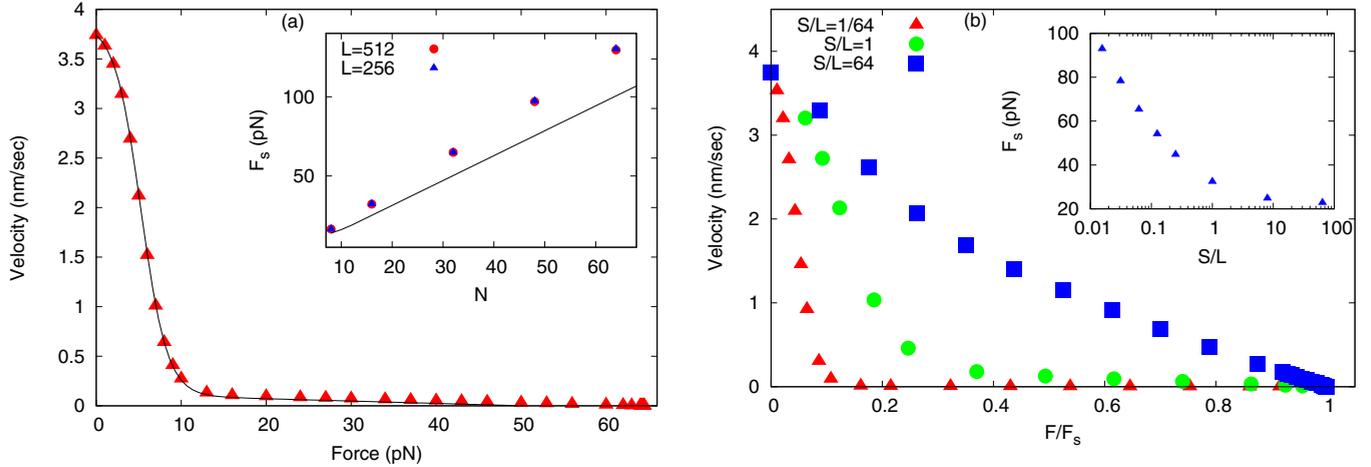
FIG. 5. Force-velocity characteristic for multiple filaments. (a) Velocity shows very slow decay for large F, when global movement can be neglected and V can be assumed to be governed by local fluctuations alone. Here, we have used $L = 512$ and $N = 32$. Inset shows stall force as a function of N for two different L values. We find stall force scales linearly with N and remains independent of L. The continuous lines show analytical results. (b) Dependence of force-velocity characteristic on the time scale of the barrier dynamics. In this case we find the same qualitative effect as in the single filament case. Here, we have used $N = 16$ and $L = 128$.

the driving rate, where the strongly driven and weakly driven regimes are separated by a minimum in the width of the membrane profile. Although the filaments only impart local drive to the membrane, and no global movement of the membrane is considered in [35], the velocity still shows an exponential dependence on the membrane tension, whereas in our model the exponential dependence is caused by the global movement and the local fluctuations generate a velocity that decreases roughly linearly with the external load.

One interesting result obtained in our system is the dependence of the qualitative shape of the F-V curve on the relative time scale between the filament polymerization and barrier fluctuation. For slow barrier dynamics, the curve has a convex shape and V shows an exponential decay for small and moderate F. But for fast barrier dynamics when the local fluctuations become more important, there is significant deviation from exponential dependence. A similar effect was reported in [21] for a hybrid mesoscopic model that combines the microscopic dynamics of semiflexible actin filaments and the viscous retrograde flow of actin network modeled as a macroscopic gel. It was shown that the force-velocity curve can be both convex and concave, depending on the characteristic time scale of recoil of the gel-like network. It is remarkable that our simple lattice gas model can reproduce this same effect, which underlines the importance of the relative time scale of obstacle and filament dynamics on the force generation mechanism.

Throughout this paper, we have considered the case $\delta = d$, when the local movement of the barrier occurs in steps whose size is equal to that of a monomer. We have verified (data not shown here) that many of our qualitative conclusions remain valid for $\delta \ll d$. In other words, even when the shape fluctuations of the barrier occur over much smaller length scales, their effect cannot be ignored. We find that the stall force continues to show dependence on the barrier properties. The relative time scales between the filament and barrier dynamics affect the F-V curve in the same way. However, the quantitative value of the stall force increases as smaller δ values are considered.

Finally, our simple model shows that a nonrigid obstacle can produce remarkable effects on force generation of parallel actin filaments. Our results underline the importance of the local shape distortions of an obstacle and indicate that more research with detailed modeling of this aspect is required. Many of our conclusions are generic and can be expected to remain valid in systems where different descriptions of a nonrigid obstacle are used. This also opens up the possibility of observing some of these effects in experiment. For example, the change of shape of the barrier with external load can be monitored in an experiment and our prediction that the height variation across the barrier increases with load can be explicitly verified. The key feature of a fluctuating barrier is that one component of velocity comes from the local fluctuations and a direct measurement of this component will surely give insights into the effects of barrier fluctuations. Our model shows that for multiple filaments close to the stalling regime, velocity is dominated by these local movements and we also predict the scaling behavior of this velocity with filament density and barrier size. It would be interesting to verify these predictions in experiments, which would not only shed light on the qualitative nature of the local fluctuations but would also provide insights about their quantitative behavior.

APPENDIX A: CALCULATION OF $p_v(i)$ AND $p_h(i)$ FOR A SINGLE FILAMENT

The shape of the barrier changes due to transition between local hills and valleys. The probability to find a hill at a site s located at a distance i from the binding site is $p_h(i)$ and
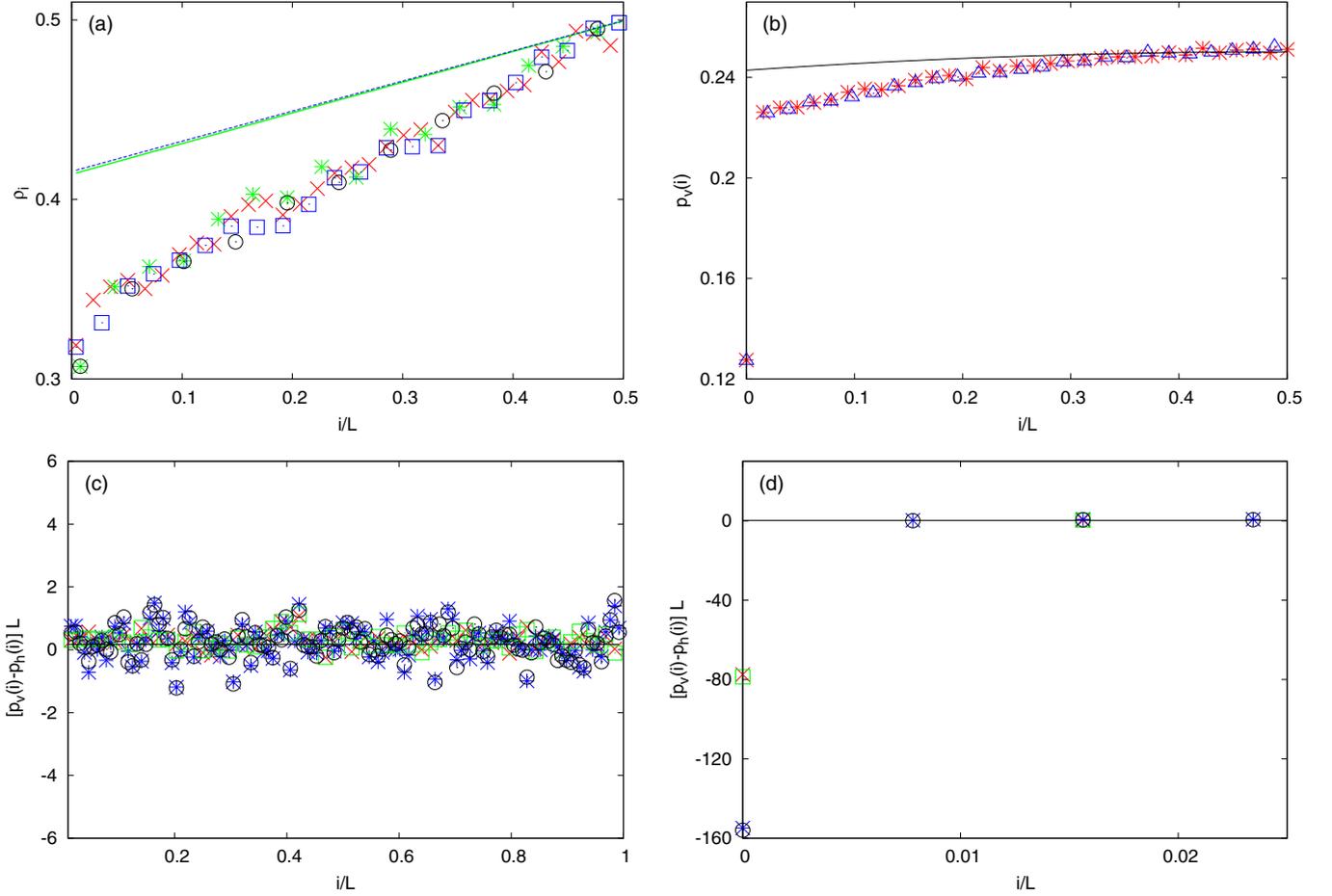
FIG. 6. Average shape of the barrier for single filament. Discrete points show simulation results and continuous lines show analytical predictions. (a) Probability ρ_i to find an upslope bond as a function of scaled distance i/L from the binding site. $\rho_i = 1/2$ for $i = L/2$ and for larger i, we have $\rho_i = 1 - \rho_{i-L/2}$. The open symbols correspond to $F = 0$ and the closed symbols correspond to $F = 4$ pN. Symbols $*$ and $\circ$ are for $L = 128$ and $\times$ and $\square$ are for $L = 256$. These data show that, except close to the binding site, ρ_i increases linearly with i with a gradient $\sim 1/L$. We also find that ρ_i remains almost the same for these F values. The continuous lines are analytical predictions, where the green solid line is for $F = 0$ and the blue dashed line is for $F = 4$ pN. (b) Probability $p_v(i)$ to find a valley at a distance i from the binding site. For $i = 0$ the probability is substantially smaller compared to the rest of the system, which means it is rather unlikely to find a valley at the binding site. The symbols $*$ and $\triangle$ represent $F = 0$ pN and 4 pN, respectively. We have used $L = 512$ here. (c) and (d) $[p_v(i) - p_h(i)]$ shows a sharp jump at $i = 0$ and then remains constant at a value that scales as $1/L$. The open symbols correspond to $F = 0$ and the closed symbols correspond to $F = 4$ pN. Symbols $*$ and $\circ$ are for $L = 256$ and $\times$ are $\square$ are for $L = 512$.

it can be written as $\rho_i(1 - \rho_{i+1})$, where ρ_i is the probability that the bond preceding the site s has $\pi/4$ orientation and $(1 - \rho_{i+1})$ is the probability that the bond immediately after the site s has $-\pi/4$ orientation. Here, we have used mean-field theory and neglected correlation between the bonds. The probability to find a valley at site s can similarly be written as $(1 - \rho_i)\rho_{i+1}$. The transition rate from a hill to a valley is R_- and the reverse process occurs with rate R_+. For $i \neq 0$, $R_+/R_- = \exp(-\beta Fd/L)$. However, when $i = 0$, or, in other words, the site s is the binding site itself, then although valley to hill transition is not affected, the reverse transition can take place only when the filament is not in contact with the binding site. We therefore make the simplifying assumption that the effect of the filament can be included by merely rescaling the hill to valley transition rate at the binding site by the probability that the filament is in contact. In Sec. III we calculate the contact probability $p_0 = 1 - W_0/U_0 \simeq 1/2$. The master equations describing the time evolution of ρ_i can then

be written as

$$\frac{d\rho_i}{dt} = (1 - \rho_i)(R_-\rho_{i-1} + R_+\rho_{i+1})$$
$$- \rho_i[R_-(1 - \rho_{i+1}) + R_+(1 - \rho_{i-1})],$$
$$\text{for } 2 \leqslant i \leqslant L - 1, \qquad (A1)$$

and at the binding site,

$$\frac{d\rho_1}{dt} = (1 - \rho_1)[R_-(1 - p_0)\rho_L + R_+\rho_2]$$
$$- \rho_1[R_-(1 - \rho_2) + R_+\rho_1(1 - \rho_L)], \qquad (A2)$$

where we have applied periodic boundary condition, which also gives

$$\frac{d\rho_L}{dt} = (1 - \rho_L)(R_-\rho_{L-1} + R_+\rho_1)$$
$$- \rho_L[R_-(1 - \rho_1)(1 - p_0) + R_+(1 - \rho_{L-1})]. \quad (A3)$$

We solve the above equations in the steady state when the left-hand sides vanish. To leading order in $1/L$, we find $\rho_i = a + bi/L$, where a and b are related via the condition $\sum_{i=1}^{L} \rho_i = L/2$ and b satisfies the quadratic equation

$$\left[\frac{\beta F d}{2L} - \frac{p_0}{4}\left(1 - \frac{2}{L}\right) \right] b^2$$
$$+ \left[1 - \frac{\beta F d}{4L} - \frac{p_0}{2}\left(1 - \frac{1}{L}\right) \right] b + \frac{1}{4}\left(\frac{\beta F d}{L} - p_0 \right) = 0,$$

$$(A4)$$

one of whose roots can be discarded from the condition that $0 \leqslant \rho_i \leqslant 1$ for all i. For a given F, therefore, ρ_i varies linearly with the distance from the binding site with a gradient $1/L$. For $F = 0$, we have $a = (\sqrt{2} - 1)$ and $b = (3 - 2\sqrt{2})$. For $0 \leqslant F \leqslant F_s$, the ranges of variation of a and b are rather small and occur at third or higher decimal places. Therefore, ρ_i does not change significantly with F. Our simulation data in Fig. 6(a) show similar qualitative behavior, although close to the binding site there is deviation of ρ_i from linearity. The quantitative values of a and b, however, do not match with simulations. We attribute this mismatch to the mean-field theoretic assumptions used in our calculation.

We calculate $p_v(i)$ and $p_h(i)$ from ρ_i and compare with simulation in Fig. 6(b). Notice that from our analytical expression for ρ_i, it follows immediately that $[p_v(i) - p_h(i)]$ is independent of i and $\sim b/L$. This has important consequence for our calculation of V_2 in Sec. III. Moreover, the probability that the filament is in contact with a valley is given by $p_v(0)p_0$ and our numerical results in Fig. 6(b) show that this probability is rather small.

APPENDIX B: VARIATION OF CONTACT PROBABILITY FOR A SINGLE FILAMENT WITH LOAD FOR FAST AND SLOW BARRIER DYNAMICS

The variation of contact probability with load is shown in Fig. 7.

APPENDIX C: CALCULATION OF CONTACT PROBABILITY FOR MULTIPLE FILAMENTS

Let N_i be the average number of filaments at a distance i from the respective binding sites. By definition, N_0 is the average number of bound filaments and the contact probability is $p_0 = N_0/N$. The time-evolution equations for N_i can be written as

$$\frac{dN_0}{dt} = U_0 N_1 - \{(N_0 - 1)U_0 e^{-\beta F d} + W_0\} N_0, \quad (C1)$$

$$\frac{dN_1}{dt} = \{(N_0 - 1)U_0 e^{-\beta F d} + W_0\} N_0 + U_0 N_2$$
$$- (N_0 U_0 e^{-\beta F d} + W_0 + U_0) N_1, \quad (C2)$$

$$\frac{dN_i}{dt} = (N_0 U_0 e^{-\beta F d} + W_0) N_{i-1} + U_0 N_{i+1}$$
$$- (N_0 U_0 e^{-\beta F d} + W_0 + U_0) N_i, \text{ for } i \geqslant 2. \quad (C3)$$

Here, we have assumed that the distance i between the filament tip and the binding site can change only due to polymerization and depolymerization dynamics and the global movement of the whole barrier due to polymerization of bound filaments. We have neglected local height fluctuations occurring at the binding sites. As we show below, this approximation works reasonably well as long as the filament density N/L is small and the time scale of barrier fluctuation is comparable to, or slower than the filament dynamics. For very fast motion of the barrier, the height fluctuations at the binding sites become more frequent and this assumption breaks down.

FIG. 7. Contact probability p_0 as a function of F for single filament. Our analytical calculation yields $p_0 = (1 - W_0/U_0) \simeq 0.5$. For slow barrier dynamics, we find reasonable agreement. But for fast barrier dynamics, our analytical prediction does not remain valid anymore and p_0 increases with F. The simulation parameters are as in Fig. 2.
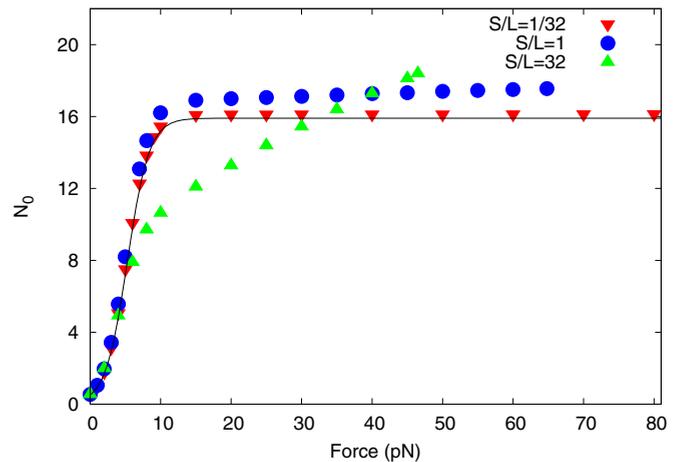
FIG. 8. Average number of bound filaments N_0 as a function of force F. For slow barrier dynamics, our analytical prediction in Eq. (C6) agrees well with numerics. But as the barrier dynamics becomes faster, deviations are observed. Here we have used $L = 256$, $N = 32$. Other simulation parameters are the same as in Fig. 2.

Solving Eqs. (C1), (C2), (C3) in the steady state, we obtain the recursion relation

$$N_{i+1} = \left(\frac{N_0 U_0 e^{-\beta F d} + W_0}{U_0} \right)^i N_1, \quad i = 1, 2, \ldots, \quad \text{(C4)}$$

and

$$N_1 = \frac{(N_0 U_0 e^{-\beta F d} + W_0 - U_0 e^{-\beta F d})}{U_0} N_0. \quad \text{(C5)}$$

Using the normalization relation, $\sum N_i = N$, we get

$$N_0 = \frac{N(U_0 - W_0)}{U_0 - U_0 e^{-\beta F d} + N U_0 e^{-\beta F d}} \quad \text{(C6)}$$

and the contact probability has the form $p_0 = \frac{(U_0 - W_0)}{U_0 + (N-1) U_0 e^{-\beta F d}}$. In Fig. 8 we compare this result with simulation and find reasonable agreement.

[1] J. Howard, *Mechanics of Motor Proteins and the Cytoskeleton* (Sinauer Associates, Sunderland, MA, 2001).

[2] T. D. Pollard and J. A. Cooper, Actin, a central player in cell shape and movement, Science **326**, 1208 (2009).

[3] L. Blanchoin, R. B. Paterski, C. Sykes, and J. Plastino, Actin dynamics, architecture and mechanics in cell motility, Physiol. Rev. **94**, 235 (2014).

[4] P. Friedl and D. Gilmour, Collective cell migration in morphogenesis, regeneration and cancer, Nat. Rev. Mol. Cell Biol. **10**, 445 (2009).

[5] Y. Marcy, J. Prost, M. F. Carlier, and C. Sykes, Forces generated during actin-based propulsion: A direct measurement by micromanipulation, Proc. Natl. Acad. Sci. USA **101**, 5992 (2004).

[6] C. Brangbour, O. du Roure, E. Helfer, D. Démoulin, A. Mazurier, M. Fermigier, M. F. Carlier, J. Bibette, and J. Baudry, Force-velocity measurements of a few growing actin filaments, PLoS Biol. **9**, e1000613 (2011).

[7] D. Démoulin, M. F. Carlier, J. Bibette, and J. Baudry, Power transduction of actin filaments ratcheting in vitro against a load, Proc. Natl. Acad. Sci. USA **111**, 17845 (2014).

[8] S. H. Parekh, O. Chaudhuri, J. A. Theriot, and D. A. Fletcher, Loading history determines the velocity of actin-network growth, Nat. Cell Biol. **7**, 1219 (2005).

[9] M. Prass, K. Jacobson, A. Mogilner, and M. Radmacher, Direct measurement of the lamellipodial protrusive force in a migrating cell, J. Cell. Biol. **174**, 767 (2006).

[10] J. Zimmermann, C. Brunner, M. Enculescu, M. Goegler, A. Ehrlicher, J. Käs, and M. Falcke, Actin filament elasticity and retrograde flow shape the force-velocity relation of motile cells, Biophys. J. **102**, 287 (2012).

[11] P. A. Giardini, D. A. Fletcher, and J. A. Theriot, Compression forces generated by actin comet tails on lipid vesicles, Proc. Natl. Acad. Sci. USA **100**, 6493 (2003).

[12] M. J. Footer, J. W. J. Kerssemakers, J. A. Theriot, and M. Dogterom, Direct measurement of force generation by actin filament polymerization using an optical trap, Proc. Natl. Acad. Sci. USA **104**, 2181 (2007).

[13] D. R. Kovar and T. D. Pollard, Insertional assembly of actin filament barbed ends in association with formins produces piconewton forces, Proc. Natl. Acad. Sci. USA **101**, 14725 (2004).

[14] C. S. Peskin, G. M. Odell, and G. F. Oster, Cellular motions and thermal fluctuations: The Brownian ratchet, Biophys. J. **65**, 316 (1993).

[15] A. E. Carlsson, Force-velocity relation for growing biopolymers, Phys. Rev. E **62**, 7082 (2000).

[16] N. J. Burroughs and D. Marenduzzo, Growth of a semiflexible polymer close to a fluctuating obstacle: Application to cytoskeletal actin fibres and testing of ratchet models, J. Phys. Condens. Matter **18**, S357 (2006).

[17] T. E. Schaus and G. G. Borisy, Performance of a population of independent filaments in lamellipodial protrusion, Biophys. J. **95**, 1393 (2008).

[18] K. Tsekouras, D. Lacoste, K. Mallick, and J. F. Joanny, Condensation of actin filaments pushing against a barrier, New J. Phys. **13**, 103032 (2011).

[19] J. Krawczyk and J. Kierfeld, Stall force of polymerizing microtubules and filament bundles, Europhys. Lett. **93**, 28006 (2011).

[20] D. Das, D. Das, and R. Padinhateeri, Collective force generated by multiple biofilaments can exceed the sum of forces due to individual ones, New J. Phys. **16**, 063032 (2014).

[21] J. Zhu and A. Mogilner, Mesoscopic model of actin-based propulsion, PLoS Comput. Biol. **8**, e1002764 (2012).

[22] R. Wang and A. E. Carlsson, Load sharing in the growth of bundled biopolymers, New J. Phys. **16**, 113047 (2014).

[23] D. K. Hansda, S. Sen, and R. Padinhateeri, Branching influences force-velocity curve and length fluctuations in actin networks, Phys. Rev. E **90**, 062718 (2014).

[24] N. S. Gov and A. Gopinathan, Dynamics of membranes driven by actin polymerization, Biophys. J. **90**, 454 (2006).

[25] E. Atilgan, D. Wirtz, and S. X. Sun, Mechanics and dynamics of actin-driven thin membrane protrusions, Biophys. J. **90**, 65 (2006).

[26] A. P. Liu, D. L. Richmond, L. Maibaum, S. Pronk, P. L. Geissler, and D. A. Fletcher, Membrane-induced bundling of actin filaments, Nat. Phys. **4**, 789 (2008).

[27] M. Kardar, G. Parisi, and Y.-C. Zhang, Dynamic Scaling of Growing Interfaces, Phys. Rev. Lett. **56**, 889 (1986).

[28] S. F. Edwards and D. R. Wilkinson, The surface statistics of a granular aggregate, Proc. R. Soc. London **381**, 17 (1982).

[29] T. D. Pollard, Rate constants for the reactions of ATP- and ADP-actin with the ends of actin filaments, J. Cell. Biol. **103**, 2747 (1986).

[30] A. Mogilner and G. Oster, The physics of lamellipodial protrusion, Eur. Biophys. J. **25**, 47 (1996).

[31] A. Mogilner and G. Oster, Cell motility driven by actin polymerization, Biophys. J. **71**, 3030 (1996).

[32] D. Das, D. Das, and R. Padinhateeri, Force-induced dynamical properties of multiple cytoskeletal filaments are distinct from that of single filament, PLoS One **9**, e114014 (2014).

[33] A. Mogilner and G. Oster, The polymerizing ratchet model explains the force-velocity relation for growing microtubule, Eur. Biophys. J. **28**, 235 (1999).

[34] A. Mogilner and G. F. Oster, Force generation by actin polymerization. II. The elastic ratchet and tethered filaments, Biophys. J. **84**, 1591 (2003).

[35] S. L. Narasimhan and A. Baumgaertner, Dynamics of a driven surface, J. Chem. Phys. **133**, 034702 (2010).